Tensile Properties of Single Desmin Intermediate Filaments

Laurent Kreplak,* Harald Herrmann,† and Ueli Aebi*
*M. E Müller Institute for Structural Biology, Biozentrum, University of Basel, 4056 Basel, Switzerland; and †Department of Molecular Genetics, German Cancer Research Center, 69120 Heidelberg, Germany

ABSTRACT Within muscle fibers, desmin intermediate filaments (IFs) are major constituents of the extrasarcomeric cytoskeleton. However, their contribution to the mechanical properties of myocytes has remained elusive. We present an experimental approach to measure the extensibility and the tensile strength of in vitro reconstituted desmin IFs adsorbed to a solid support. The tip of an atomic force microscope (AFM) was used to push on single filaments perpendicular to the filament axis. The torque of the AFM cantilever was monitored during the pushing events to yield an estimate of the lateral force necessary to bend and stretch the filaments. Desmin IFs were stretched up to 3.4-fold with a maximum force of ~3.5 nN. Fully stretched filaments exhibited a much smaller diameter than did native IFs, i.e., ~3.5 nm compared to 12.6 nm, both by AFM and electron microscopy. Moreover, we combined the morphological and lateral force data to compute an average stress-strain curve for a single desmin filament. The main features were a pronounced strain-hardening regime above 50% extension and a tensile strength of at least 240 MPa. Because of these nonlinear tensile properties, desmin IFs may dissipate mechanical energy and serve as a physical link between successive sarcomeres during large deformation.

INTRODUCTION

Intermediate filaments (IFs) constitute, together with microfilaments (MFs) and microtubules, the cytoskeleton of all metazoan cells. In contrast to MFs and microtubules, which are made from globular proteins, i.e., actins and tubulin, respectively, the subunit proteins of IFs are elongated coiled-coils that are oriented along the filament axis exhibiting extensive intermolecular ionic and hydrophobic interactions between individual subunits (1). These molecular properties are thought to be the reason for the resistance of IFs against buffers of high ionic strength and nonionic detergent. Moreover, it has been suggested that IFs are involved in important tissue-specific mechanical functions in cells and tissues (2). This was first recognized with keratins, where a single mutation in one of the basal cell keratins causes the mechanical disruption of the entire cell layer upon application of mechanical stress.

Similarly, in the case of vertebrate skeletal and cardiac muscles, where desmin IFs form a three-dimensional filament lattice around the myofibrils, the inactivation of the desmin gene in mice indicated that desmin IFs execute an important function in buffering stress (3). Short desmin IFs laterally connect the Z-disks of adjacent myofibrils to maintain their longitudinal register (4,5), whereas longer filaments connect successive Z-disks along the same myofibril (3,6). Desmin IFs also link the Z-disks to costameres and desmosomes at the periphery of the muscle fiber, thus contributing to the mechanical integrity of muscle tissue (7). However, the exact role of this desmin continuum in force transmission and in susceptibility to injury has remained elusive (8). The response of desmin wild-type and null mouse muscles to various mechanical insults like eccentric contractions (9) and intensive exercise (10) has yielded conflicting results (3). The interpretation of these in vivo mechanical data was complicated by the current lack of quantitative biophysical data on desmin IFs, especially regarding their tensile properties (8,11).

IFs are flexible filaments with an average diameter of 10 nm and a persistence length of only 1 μm (12). We and others have recently demonstrated that IFs can be stretched up to 3.5-fold (250% extension) before they rupture (13,14). The molecular origin of this extensibility resides in the elementary building block of IFs, i.e., the α-helical coiled-coil dimer that can be converted into β-sheet-type structures upon stretching (14,15; reviewed in Kreplak and Fudge (11)). However, the force necessary to fully stretch a single IF has not been measured yet (11). To achieve this goal, we developed an atomic force microscopy (AFM) approach whereby single desmin IFs, adsorbed to a solid support, were stretched by the AFM tip in a physiological buffer environment (13). The change in torque of the AFM cantilever was monitored during stretch, yielding an estimate of the applied lateral force.

AFM imaging revealed the stretched filaments to remain adsorbed to the surface and to not significantly relax. Hence it was possible to directly monitor the change in morphology of each filament, i.e., the extension of filament length and reduction in diameter. The structural and mechanical data extracted from each stretching event were merged into an approximate stress-strain curve for a single desmin filament. The main features of the tensile properties of a desmin IF are a yield stress of ~10 MPa, a strain-hardening behavior that becomes prominent above 50% extension, an extensibility of 240%, and a tensile strength of at least 240 MPa after cor-

Submitted August 21, 2007, and accepted for publication November 28, 2007.

Address reprint requests to Laurent Kreplak, Assistant Professor, Department of Physics and Atmospheric Science, Dalhousie University, Halifax, NS B3H 3J5, Canada. Tel.: 902-494-84-35; Fax: 902-494-51-91; E-mail: kreplak@fizz.phys.dal.ca.

Editor: Denis Wirtz.

0006-3495/08/04/2790/10 $2.00

doi: 10.1529/biophysj.107.119826

rection for friction between the filaments and the surface. A single filament was also able to dissipate at least 40 MJ/m^3 of mechanical energy. Based on these results and taking into account the topology of the desmin network in vivo, the contribution of desmin IFs to the mechanical response of muscle tissue should depend dramatically on the strength and orientation of the applied deformation.

MATERIALS AND METHODS

Desmin preparation and assembly

Human and murine recombinant desmin were obtained as described and stored at −80°C in DP buffer (5 mM Tris-HCl, pH 8.4, 1 mM dithiothreitol) containing 8 M urea, 1 mM EDTA, 0.1 mM EGTA, and 10 mM methyl ammonium chloride (16). The day before use, the protein was diluted to 1 mg/ml with the above storage buffer, followed by step-wise dialysis at room temperature into DP buffer containing 6 M, 4 M, 2 M, and 0 M urea. Dialysis was continued overnight at 4°C into fresh DP buffer without urea. Desmin forms stable tetramers in DP buffer, as reported previously (17). For the AFM experiments, assembly of murine desmin was induced by adding an equal volume of 45 mM Tris-HCl (pH 7.0), containing either 100 or 200 mM NaCl, to a DP solution containing 0.1 mg/ml desmin. The final protein concentration was 0.05 mg/ml. After 1 h at 37°C, assembly was terminated by adsorption of a 10 μl aliquot to a freshly cleaved mica disk for 5 s, before washing with 25 mM Tris-HCl buffer, pH 7.5, containing 50 or 100 mM NaCl, respectively. For the electron microscopy (EM) experiments, assembly of human or murine desmin was induced by adding either an equal volume of 45 mM Tris-HCl buffer, pH 7.0, with 100 mM NaCl or a 1/10 volume of 200 mM Tris-HCl buffer, pH 7.0, with 500 mM NaCl to a desmin solution (0.6, 0.8, or 1 mg/ml) in DP, followed by incubation at 37°C for 1 h.

Electron microscopy of sheared IF networks

After assembly, a 10 or 20 μl drop of desmin filaments was adsorbed to a Teflon surface. A glow-discharged carbon-coated copper grid was placed on top of the drop and pulled horizontally 30 mm in 10 s to totally shear and rupture the desmin network. Then the grid was removed, washed with water, and stained with 2% uranyl acetate. EM pictures were recorded with a Hitachi H-7000 transmission electron microscope (Hitachi, Tokyo, Japan) operated at 100 kV.

Atomic force microscopy

All samples were imaged in contact mode in liquid using a Nanowizard AFM (JPK, Berlin, Germany) with a closed-loop scanner. The rectangular silicon cantilevers were 220 μm long, 20 or 45 μm wide, with an oxide sharpened tip at one end (type LFM and PPP BSI from Nanosensors, Neuchatel, Switzerland). The exact dimensions of the cantilevers, including their thickness, and the height of the pyramidal tips were measured by scanning EM. The normal spring constant of each cantilever was measured using the peak frequency f_0 and the quality factor Q of the noise spectrum acquired in air (18). The dimensions of the cantilever and the shear modulus of silicon $G = 50$ GPa were used to estimate the lateral spring constant (19). The cantilevers had a vertical spring constant $C_Z = 0.025$–0.04 N/m and lateral spring constant $C_L = 3$–7.5 N/m. Before each series of manipulations, the vertical sensitivity S_Z was measured in nm/V on a corresponding vertical force versus tip displacement curve. The lateral sensitivity S_L was estimated using the formula $S_L = 3/2 \times h/l \times S_Z$ for a rectangular cantilever of length l with a tip height h.

Stretching protocol

Before laterally pushing on single desmin filaments adsorbed to mica in buffer, we imaged an area of 100 or 400 μm^2 at a constant vertical force of 0.1 nN and a scanning speed of 1–2 Hz to preserve the filament architecture (Fig. 1 *A*). The scanning angle was chosen such that the rectangular cantilever was perpendicular to the fast scan axis. Then the tip was withdrawn, and single filaments were stretched using the stored AFM image as a reference. This was possible due to the closed-loop scanner that allowed us to reliably address every single pixel of the image. For each stretching experiment, the tip was moved from left to right along a horizontal line crossing a desmin

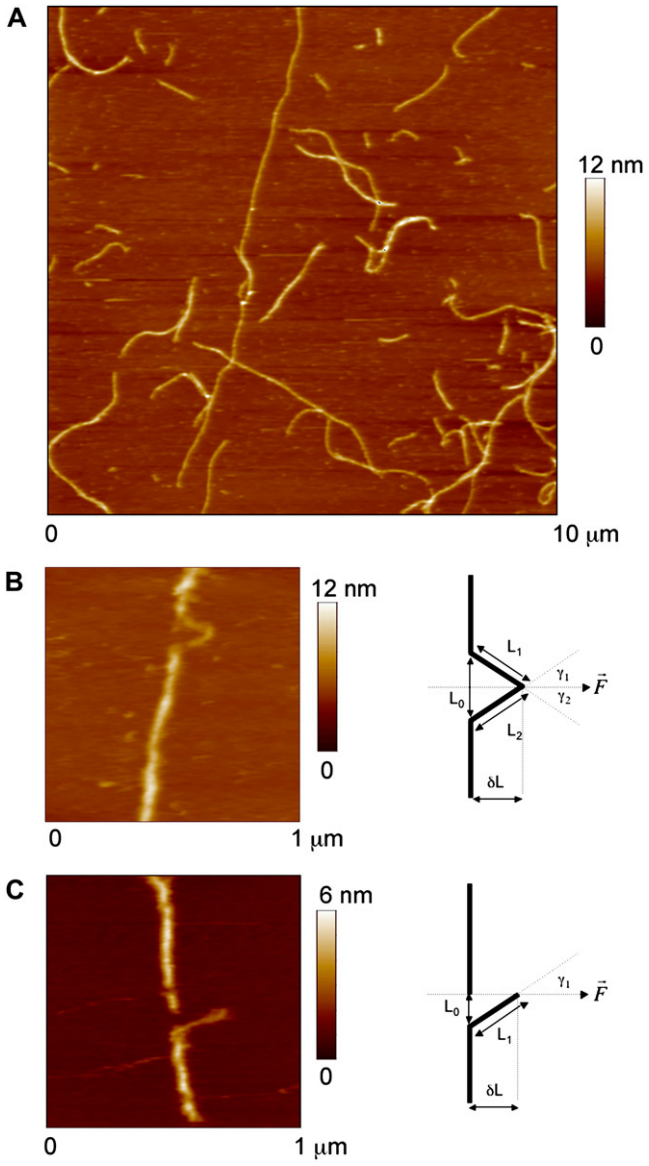

FIGURE 1 Murine desmin filaments, at a concentration of 0.05 mg/ml, were assembled for 1 h at 37°C in 25 mM Tris-HCl (pH 7.5), 100 mM KCl, and adsorbed to freshly cleaved mica. (*A*) Contact mode AFM image. (*B*) AFM image of a stretched desmin filament where two branches are visible. (*C*) AFM image of a ruptured and stretched desmin filament where only one branch is visible. For each AFM image, a diagram presents the geometrical parameters measured on the AFM images after stretching. $\vec{F}$ represents the force vector applied by the AFM tip to the filament. $\vec{F}$ was always parallel to the fast scanning axis and oriented from left to right. L_1 and L_2 are the lengths of the stretched branches. γ_1 and γ_2 are the angles between the branches and $\vec{F}$. δL is the distance by which the filament was moved by the tip.

filament at a speed of 50 nm/s. During the experiment, the vertical force applied by the cantilever to the surface (the vertical deflection) was fixed between 1 and 7 nN to laterally push the filament. At the same time the vertical and lateral deflection of the cantilever and the height with respect to the surface were recorded as a function of the tip position at a sampling rate of 100 Hz. Upon completion of a single-filament stretching experiment, the event area was imaged again at a constant vertical tip force of 0.1 nN and a scanning speed of 1–2 Hz to document the ''irreversible'' deformation caused by the lateral pushing event previously mediated through the action of the AFM tip (Fig. 1 *B*).

Data analysis

The AFM images were analyzed with Image SXM (http://www.liv.ac.uk/~sdb/ImageSXM/). When a segment of filament was stretched to yield either one or two branches (Fig. 1, *B* and *C*), we measured the filament displacement by the tip δL, the height of the stretched branches H_S, the height of the unstretched filament H_0, the length of the filament segment before deformation L_0, the lengths of the stretched filament branches L_1 and L_2, and the angle between the filament axis and the tip scan line γ. When the filament was stretched to yield two branches (Fig. 1 *B*, *right*), we measured the two angles γ_1 and γ_2 and calculated the effective $\cos\gamma$, i.e., $(\cos\gamma_1 + \cos\gamma_2)/2$. The extension of a stretched filament segment was calculated as $\varepsilon = 100 \times ((L_1 + L_2)/L_0 - 1)\%$.

In parallel, the corresponding lateral deflection trace was analyzed using Origin 6.0. The lateral deflection was transformed into a lateral force using the lateral sensitivity and the lateral spring constant (see the section ''Atomic force microscopy''). The friction between the tip and the surface gave rise to background noise with an average amplitude of 0.4 nN that was fitted by a straight line and subtracted. The initial contact point between the tip and the filament was estimated on the lateral force trace and used as the origin. The lateral force traces were smoothened using a five-point averaging algorithm. Then the filament displacement by the tip, δL (Fig. 1, *B* and *C*), was estimated a second time along with the maximum lateral force applied to the filament, F_{max} [nN], and the mechanical energy, E [nN·nm], that was dissipated during the stretching event. Notice that the values for δL—i) directly estimated from an AFM image of a stretched filament segment, and ii) determined from the corresponding lateral force versus tip displacement curve—were very similar (data not shown). This indicated that little relaxation of the stretched filament segment occurred after lateral pushing by the AFM tip. Hence the extension ε measured on the image is a good approximation of the maximum length increase of a given filament segment.

RESULTS

Stretching assay

Desmin was assembled routinely at a concentration of 0.05 mg/ml for 1 h at 37°C in 25 mM Tris-HCl buffer, pH 7.5, containing 100 mM NaCl and adsorbed to freshly cleaved mica. Contact mode AFM images at a constant vertical tip force of 0.1 nN revealed desmin filaments (Fig. 1 *A*) with a broad length distribution, an average height H_0 of 4.5 ± 0.8 nm ($n = 60$), and a full width at half-maximum of 45 ± 15 nm ($n = 60$). To stretch a desmin filament adsorbed to mica by laterally pushing it by the AFM tip, the AFM tip was moved along a path crossing the filament at a speed of 50 nm/s. The contact between the tip and the surface was controlled by applying a vertical tip force between 1 and 7 nN. A manipulation was considered successful if a visible change in shape or indent was observed afterward on the AFM image (Fig. 1 *B*).

For vertical tip forces of 1–2 nN, the filaments did not show any indent after an encounter with the tip. This was observed for filaments assembled in the presence of 50 (Fig. 2) and 100 mM NaCl (data not shown). The filaments were accurately contoured, as depicted from the height profile recorded during the tip movement across the filament (Fig. 2 *A*, *gray curve*). The contact between the tip and the filament induced a slight, measurable lateral deflection, or torsion, of the cantilever above the background noise level (Fig. 2 *A*, *black curve*). The lateral force peak and the height peak almost perfectly matched, indicating that the observed increase in lateral force was due to the encounter of the tip with the filament (Fig. 2 *A*). Repeating the same experiment two more times on the same scan line at a vertical tip force of 1 nN did not significantly change the lateral force and the height profiles presented in Fig. 2 *A*. However, a fourth experiment at a vertical tip force of 2 nN yielded a smaller height peak and a rather different lateral force profile (Fig. 2 *B*, *black curve*). The lateral force reached 1 nN, compared to 0.3 nN for the

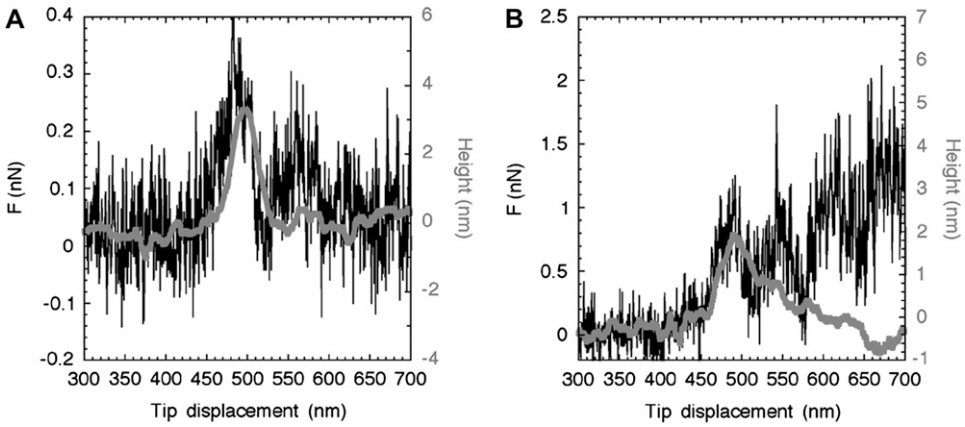

FIGURE 2 Murine desmin filaments, at a concentration of 0.05 mg/ml, were assembled for 1 h at 37°C in 25 mM Tris-HCl (pH 7.5), 50 mM KCl, and adsorbed to freshly cleaved mica. (*A*) Lateral force (*black line*) and tip height (*gray line*) recorded while laterally pushing a desmin filament at a vertical tip force of 1 nN and a scanning speed of 50 nm/s. The experiment was repeated two more times, yielding no significant change in the profiles. Notice that the increase in lateral force coincides with an increase in tip height. (*B*) Lateral force (*black line*) and tip height (*gray line*) recorded while laterally pushing the same filament at a vertical tip force of 2 nN and a scanning speed of 50 nm/s. This time a piece of detached filament remained attached to the tip. As a consequence, the lateral force did not go back to zero after the tip-filament encounter.

three previous manipulations, and the lateral force did not decrease back to the background level, indicating something remained attached to the tip (Fig. 2 *B*, *black curve*). The AFM image recorded after the last experiment revealed a clear cut along the path of the tip with no sign of stretching (data not shown). Taken together, this series of four experiments indicated that for a lateral force below 0.3 nN the filaments can be contoured several times without damage.

In contrast, for vertical tip forces between 3 and 7 nN, the filaments were always damaged by the encounter with the tip. A height peak similar to that seen in Fig. 2 *A* was rarely observed, indicating that the tip was pushing the filament rather than contouring it. We further analyzed only the stretching events resulting from one experiment, and the corresponding lateral force profile had to decrease to zero—far from the first tip-filament contact. Hence, we conclude that stretching events are more likely to be observed above a vertical tip force threshold of 2–3 nN.

Lateral force curves and the impact of transverse stretching on filament morphology

The stretching events were divided into two categories based on the resulting filament morphology: i), filament segments that were stretched to yield two branches of similar lengths (Fig. 1 *B*, *left*); and ii), filament segments that were stretched and ruptured to yield one branch (Fig. 1 *C*, *left*). The first scenario corresponded to the case where the tip indented a filament segment at its midpoint so that both halves bent and stretched in a similar way. The second scenario corresponded to the case where the tip locally ruptured the filament so that one end of the torn filament remained attached to the tip. In both cases the filament was stretched until being ruptured or until the contact between the filament and the tip was broken. After transverse stretching, each filament was imaged (Fig. 1, *B* and *C*) to measure the extent of the applied deformation. For each event, the initial length of the filament segment L_0 and the apparent extension ε were measured (Fig. 1, *B* and *C*).

We analyzed in detail a set of 60 stretching events, 34 with one branch and 26 with two branches, recorded with a vertical tip force of 3, 5, or 7 nN. The length of the filament segment L_0 varied between 35 and 140 nm, with an average value of 80 nm. There was no correlation between the vertical tip force and L_0. The extension ε, calculated from the AFM images, varied between 8% and 240% with an average value of 100%. The maximum extensibility was in good agreement with our previous AFM measurements, which were performed on single human desmin filaments (13).

Even though each stretching event was unique, the lateral force versus tip displacement curves had common features. The first encounter between the tip and the filament (Fig. 3, *A–D*) was characterized by a linear increase of the lateral force with a slope varying between 0.006 and 0.12 N/m (Fig. 3, *A–D*). Then, above a lateral force threshold between 0.8 and 3 nN, the slope of the curve decreased to almost zero (Fig. 3, *A–C*) or became negative (Fig. 3 *D*). This behavior may be interpreted as a yield due to tension building up along the filament. In most cases, corresponding to an apparent extension above 50%, the yield region was followed by an increase in slope (Fig. 3, *B–D*) due to further stretching of the filament. The amount of filament displacement by the tip was estimated as the distance δL from the first encounter of the tip and the filament to the point where the lateral force started to decrease back to zero (Fig. 3 *B*). Accordingly, δL varied between 60 and 260 nm with an average value of 150 nm.

The next step was to assemble the individual measurements into a ''master curve''. First, we plotted the maximum lateral force F_{max} and the dissipated mechanical energy E as a function of the extension ε (Fig. 4, *A* and *B*). Both parameters increased with the extension; however the trend was clearer for the energy than for the maximum lateral force. As this first analysis did not take into account the morphological changes occurring to the stretched filament and the detailed geometry of each stretching event, we characterized these in two ways. For each event, we computed the ratio of the stretched filament height H_S to the initial filament height H_0 and we estimated the angle γ between the stretched filament axis and the direction of applied deformation (Fig. 1 *C*). The ratio H_S/H_0 was used to estimate the reduction of the filament diameter upon stretching (Fig. 4 *C*). The observed decrease was faster than estimated from a constant volume approximation (Fig. 4 *C*, *dashed line*). This behavior was indicative of a decrease in the filament's volume upon stretching, typical for a plastic deformation. Upon stretching, the diameter reduction was also correlated with an alignment of the filament along the direction of applied deformation (Fig. 4 *D*).

Average tensile properties

The tensile force arising along the filament axis due to the applied lateral force can be estimated as $T = F_{max}\cos\gamma$ (Fig. 1, *B* and *C*). T was plotted as a function of the extension (Fig. 5 *A*). For clarity, the data points were averaged with a bin size of 20%. The bins containing less than three points were not averaged, and the bars correspond to standard deviations (Fig. 5 *A*). The tensile force had an apparent discontinuity, around 150% extension, from a low force regime centered at ~1 nN to a high force regime at ~3 nN (Fig. 5 *A*).

The dissipated mechanical energy per unit volume was estimated for each event as the mechanical energy E (Fig. 4 *B*) divided by the volume of the filament piece that was stretched $V_{fil} = \pi R_0^2 L_0$, where R_0 is the unstretched filament radius which was estimated to 6.3 nm in a previous scanning transmission electron microscopy (TEM) study (17). The data points were averaged with a bin size of 20%. The mechanical energy per unit volume stayed more or less constant (~10 MJ/m^3) up to ~100% extension followed by a steep increase up to 50 MJ/m^3 at 240% extension (Fig. 5 *B*).

Last but not least, the tensile stress was estimated for each event as the tensile force T divided by the area S of the fila-

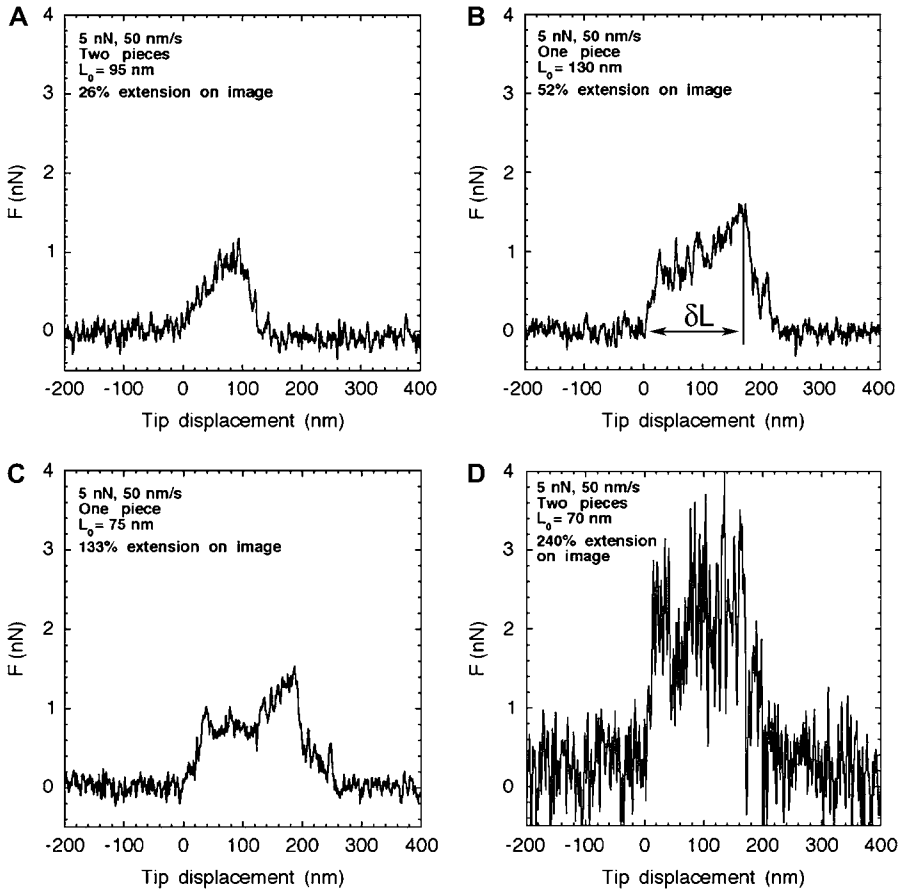

FIGURE 3 Murine desmin filaments, at a concentration of 0.05 mg/ml, were assembled for 1 h at 37°C in 25 mM Tris-HCl (pH 7.5), 100 mM KCl, and adsorbed to freshly cleaved mica. Lateral force traces during manipulation are presented for four stretching events selected from a set of 60 measurements. (*A*) The filament segment was stretched by 26% to yield two branches. A plateau is reached around 0.8 nN. (*B*) The filament segment was stretched by 52% to yield one branch. (*C*) The filament segment was stretched by 133% extension to yield one branch. In (*B*) and (*C*) the lateral force reached a plateau around 0.8 nN, which was followed by a further increase to ~1.4 nN before the tip snapped away from the filament. (*D*) The filament segment was stretched by 240% to yield two branches. In this case, the lateral force reached 3 nN before decreasing to 1 nN.

ment's cross section. Since the diameter of the filament was shown to decrease with the extension (Fig. 4 *C*), we estimated *S* in two ways. As a first approximation, we assumed that the volume of the filament remained constant, thereby yielding $S_1 = \pi R_0^2/(1+\varepsilon/100)$ where ε is the extension in percentage (Fig. 6, *filled black circles*). Then we used the experimentally determined ratio H_s/H_0 (Fig. 4 *C*) as a better estimate of the ratio R_s/R_0, where R_s is the radius of the stretched filament, yielding $S_2 = \pi R_0^2 \times (H_S/H_0)^2$ (Fig. 6, *filled gray diamonds*). Both curves exhibited a similar behavior below 100% extension with a plateau around 10 MPa. However, above 100% extension, the constant volume approximation significantly underestimated the stress applied to the filament (Fig. 6). In other words, single desmin filaments seem to strain harden when extended above 100% extension.

Transmission electron microscopy of sheared desmin networks

Based on the AFM measurements, single desmin filaments exhibited rather nonlinear tensile properties (Fig. 6) that correlated with an unusual decrease in their diameter upon stretching (Fig. 4 *C*). Using the smallest ratio of H_S/H_0, i.e., ~0.3, we estimated the minimal diameter of a fully stretched desmin filament to be 3.75 nm. Because such a small diameter could not be resolved with the AFM tips used in this study, we decided to image stretched filaments by TEM. For this purpose, human desmin at a concentration of 0.3–0.8 mg/ml was assembled for 1 h at 37°C in 25 mM Tris-HCl buffer, pH 7.5, with 50 mM NaCl. Next, a drop containing the entangled filaments was sheared between a Teflon surface and a glow-discharged carbon-coated copper grid. The filaments still adsorbed to the grid after shearing were negatively stained and imaged by EM. Most of the filaments remained undisturbed by the large shear strain applied. However, a few filaments revealed a continuous decrease in diameter (Fig. 7 *A*, *arrowheads*). This was attributable to a large tension applied to these filaments. Furthermore, in some places, the shear strain induced alignment of the filaments in the direction of the shear. Some of the thus aligned filaments exhibited diameters decreasing down to 3–4 nm (Fig. 7 *B*, *arrowheads*). Hence, also under these conditions desmin IFs were thinned to a similar value. This indicates that IFs are able to dramatically reduce their diameter without breaking.

DISCUSSION

Three-point bending test of a desmin filament adsorbed to a surface

We decided to take advantage of the inherent adhesiveness of IFs (20) to measure their tensile properties when adsorbed to a

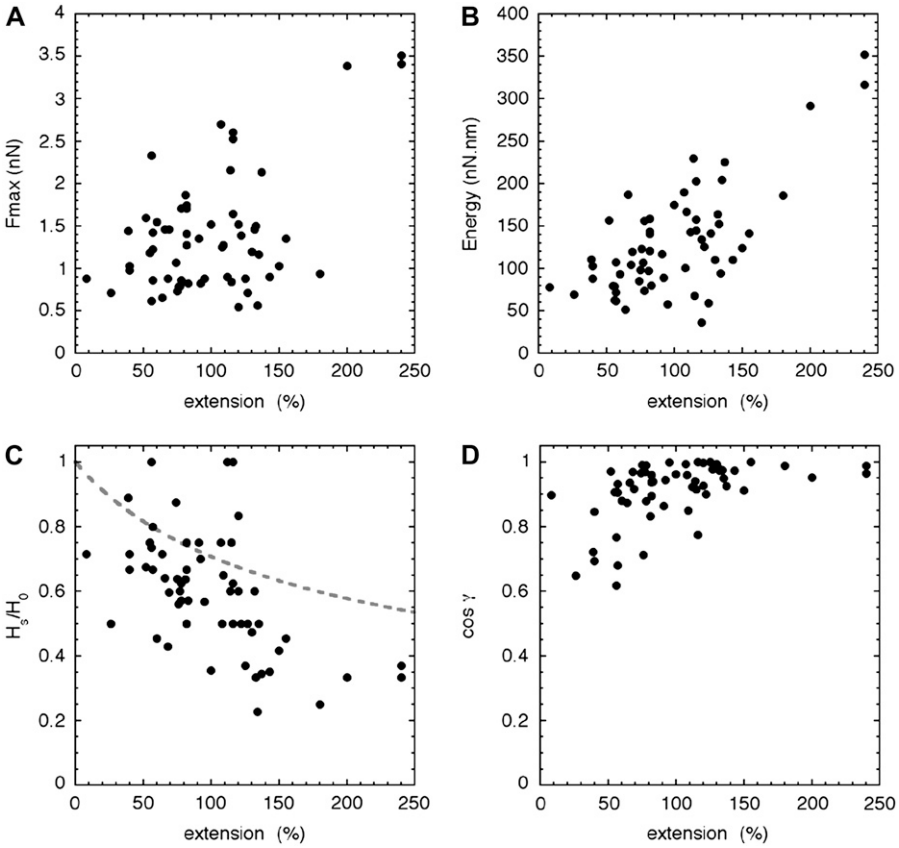

FIGURE 4 Summary of 60 different stretching events recorded on mica for desmin IFs in 25 mM Tris-HCl (pH 7.5), 100 mM NaCl. (*A*) Lateral force F_{max} in nN as a function of the extension measured on the image. (*B*) Dissipated mechanical energy in nN·nm as a function of the extension. The energy was estimated by integrating the lateral force traces between 0 and L_s (Fig. 3 *B*). (*C*) Ratio of the stretched filament height to the unstretched filament height, H_S/H_0, as a function of extension. The dashed line corresponds to the behavior of a filament stretched at a constant volume. (*D*) Cosine of the angle γ (Fig. 1 *C*) as a function of extension. At large deformation the stretched filament aligns with the axis of the applied constraint.

surface. The geometry of our experimental setup (Fig. 1, *B* and *C*) was equivalent to a three-point bending test where a filament clamped at both ends is bent by a point load applied to it in the middle (Fig. 8, *step 1*) (21,22). In the case of an elastic filament of suspended length L_0, the deflection δL in the middle (Fig. 1, *B* and *C*) increases linearly with respect to the applied lateral force F following the relation $\delta L \sim F \times L_0^3$ (Fig. 8, *step 2*) (22). When the deflection becomes significantly larger than the filament's radius (Fig. 8, step 3), there occurs a transition from pure bending to stretching and the lateral force versus tip displacement curve is dominated by the tensile properties of the filament (Fig. 8, *steps 3* and *4*) (22).

In our case, the filament is adsorbed and not clamped to a surface. Hence the length L_0 over which the bending should occur is not a priori defined. It will depend on the size of the object that is used to apply the point load, i.e., the AFM tip diameter, the local friction coefficient of the filament-surface contact, and the local bending properties of the filament. Experimentally, we observed L_0 values ranging between 35 and 140 nm. This variation cannot be due only to a change in tip-shape since the full width at half-maximum of the fila-

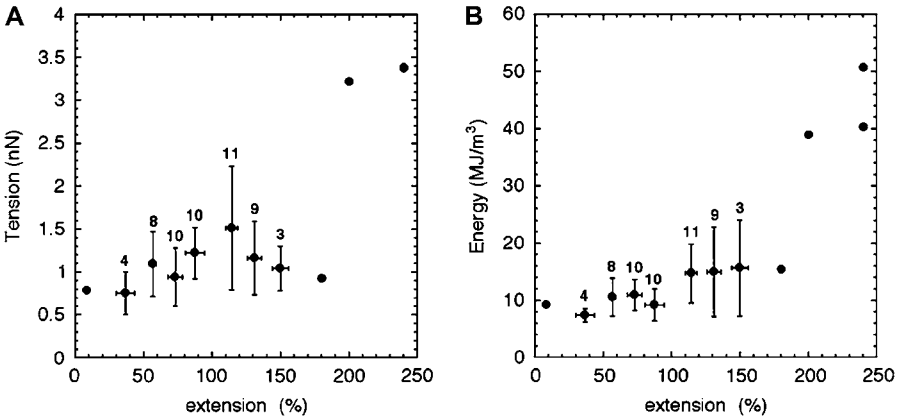

FIGURE 5 Average tensile behavior of a single desmin filament adsorbed to freshly cleaved mica in 25 mM Tris-HCl (pH 7.5), 100 mM NaCl. The data points were averaged with a bin size of 20% extension. For each bin, the mean and standard deviations and the number of events per bin are presented. For less than three events in a given bin, all the points are presented. (*A*) Tensile force $T = F_{max}\cos\gamma$ as a function of extension. (*B*) Dissipated mechanical energy per filament unit volume as a function of extension. Two regimes are visible: a plateau at 10 MJ/m^3 below 100% extension followed by a steep increase to 50 MJ/m^3 at 240% extension.

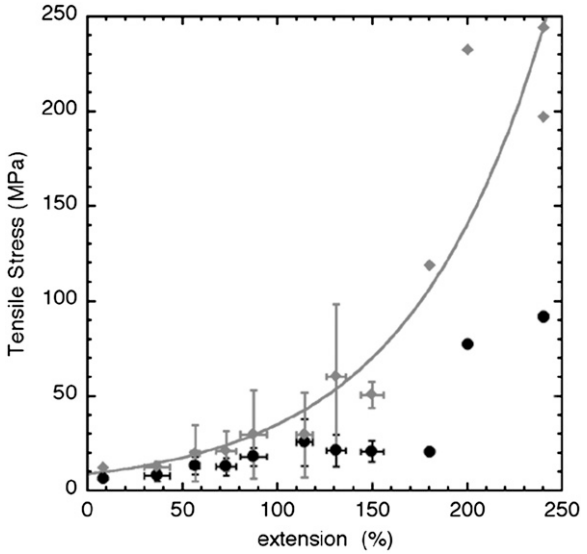

FIGURE 6 Average stress-strain curves of a single desmin filament adsorbed to mica in 25 mM Tris-HCl (pH 7.5), 100 mM NaCl. The data points were averaged with a bin size of 20% extension. For each bin the mean and standard deviations are presented. The number of events per bin is the same as in Fig. 5 *A*. The stress was computed using the average force extension curve shown in Fig. 5 *A*. The initial diameter of the filament was set to be 12.6 nm (17). The decrease of the filament's diameter upon stretching was accounted for in two ways. The filled black circles represent the stress-strain curve computed for a filament that was assumed to be stretched at constant volume. The filled gray diamonds represent the stress-strain curve taking into account the height reduction measured by AFM (Fig. 4 *C*). At up to ~100% extension both regimes yielded a relatively constant tensile stress of 10–15 MPa. Above 100%, the constant volume approximation yields a slow increase of the tensile stress to ~90 MPa at an extension of 240%. Based on the height measurements we obtained an exponential increase of the tensile stress to 200–240 MPa at an extension of 240%. The gray diamond curve was fitted with the relation $8.75 \times \exp(\varepsilon/72)$ MPa, $R = 0.93$, where ε is the extension in percentage (*gray curve*).

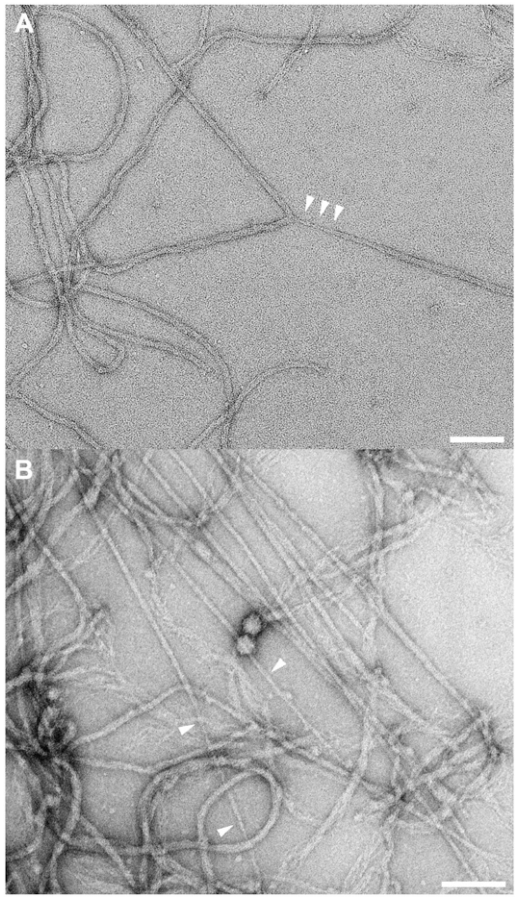

FIGURE 7 Networks of desmin filaments were assembled for 1 h at 37°C in 25 mM Tris-HCl (pH 7.5), 50 mM NaCl. After assembly, a 10 or 20 μl aliquot of desmin filaments was adsorbed to a Teflon surface, yielding a spherical drop. A glow- discharged carbon-coated copper grid was placed on top of the drop and moved horizontally by 30 mm to shear and rupture the desmin network. (*A*) TEM picture of murine desmin filaments at 0.3 mg/ml. All the filaments are undisturbed except one Y-shaped branch, where one of the filaments yields a strongly decreasing diameter (minimum around 6 nm: see *arrowheads*). (*B*) TEM picture of human desmin filaments at 0.8 mg/ml. The image depicts the tip of a strongly bundled network of filaments. Some of the filaments have diameters decreasing continuously to 3–4 nm (see *arrowheads*). Bars, 100 nm.

ments (45 ± 15 nm) did not vary much. We also observed a large variation in the bending stiffness ranging between 0.006 and 0.12 N/m with no clear dependence on L_0. This may relate to the kind of AFM tips used in this study as they had a diameter similar to the length of desmin's basic building block, i.e., the 45-nm-long dimer. Since the friction coefficient should not vary on the surface, it is most likely that the fluctuations in bending stiffness were due to local changes in the filament architecture. Hence, we may use the lower boundary of the bending stiffness, i.e., 0.006 N/m, as a rough estimate of the friction force per unit length acting on the filament. This value is in the range of what has been estimated for tobacco mosaic virus rods adsorbed to graphite and bent under ambient conditions (23).

For lateral forces below 0.3 nN, desmin filaments were contoured without any visible damage (Fig. 2 *A*). This is consistent with the reversibility range observed recently for vimentin filaments suspended over 250-nm-wide holes (21). Above that lateral force threshold, the displacement of the AFM tip induced an ''irreversible'' morphological change (Fig. 1, *B* and *C*). Accordingly, the lateral force curves exhibited either a plateau around 0.8–1 nN (Fig. 3, *A–C*) or a decrease in lateral force from up to 3 nN down to 0.8–1 nN (Fig. 3 *D*). This kind of behavior is typical for a yield regime due to strong tension arising in the filament (Fig. 8, *step 3*). This hypothesis is corroborated by the shape of stretched filaments that yield very straight branches (Fig. 1, *B* and *C*) as expected for a flexible wire under tension (24).

Taking into account the estimated friction force per unit length (see above) and the average length of the segments (i.e., 80 nm), we estimated the yield force characteristic of desmin filaments to be in the range of 0.3–0.5 nN. The large initial lateral forces measured in some cases were followed by a sudden steep decrease (Fig. 3 *D*). This behavior may be attributed to a local increase in adhesion between the filament and the surface.

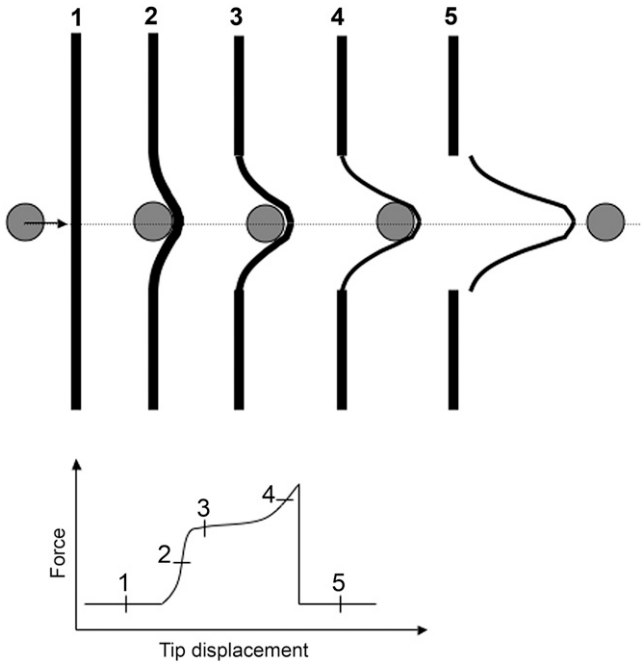

FIGURE 8 Scheme describing the main events happening during a lateral pushing experiment. (*Step 1*) The AFM tip is depicted as a gray disk and the desmin filament as a black rod. (*Step 2*) The tip-filament encounter is associated with filament bending and steep increase in the lateral force experienced by the cantilever. (*Step 3*) When the filament is deflected more than its radius, there is a transition from pure bending to stretching. The radius of the filament starts to decrease due to stretching. At that point the filament yields as seen by a plateau in the lateral force-displacement curve. (*Step 4*) The yield is followed by another increase in the force that is associated with a strong decrease of the filament's radius. This phenomenon is called ''strain hardening''. (*Step 5*) After the rupture of the filament, the AFM tip is releasing the filament by jumping over it and continues its movement. The stretched filament segment remains adsorbed to the surface. The end of the tip-filament contact is associated with a steep drop of the lateral force back to the background level.

When the mechanical deformation was large enough, i.e., above 50% extension, the yield regime was followed by a steep lateral force increase (Figs. 3, *B–D*, and 8, *step 4*). Such a nonlinear behavior was also visible when the dissipated mechanical energy per filament unit volume was plotted as a function of filament extension (Fig. 5 *B*). In this case, the yield regime corresponded to a plateau at $\sim$10 MJ/m^3 up to $\sim$100% extension followed by a steep increase up to $\sim$50 MJ/m^3. The assumption that the energy dissipated by the friction of the filament on the mica surface was much greater than the energy of the yield regime led to an underestimate of the filament energy dissipation capacity of 40 MJ/m^3 at 240% extension. For comparison, a single 100-nm-long actin filament can dissipate only $\sim$0.5 MJ/m^3 of mechanical energy before breaking (25).

Nanoscale plasticity of desmin filaments

Based on previous mechanical and structural studies of macroscopic fibers built of keratin IFs (14,15,26), it has been proposed that single IFs when stretched by more than 30% may exhibit nonlinear tensile properties associated with a plastic deformation. Elasticity is characterized by a reversible deformation, whereas plasticity is characterized by an irreversible change in volume of the material upon mechanical deformation. With our AFM setup, any visible deformation is irreversible because relaxation processes are by and large hindered by the adhesive solid support (see ''Data analysis'' section and Fig. 8, *step 5*). However, because we could accurately record the height profile of the filaments after deformation, we could directly document a decrease in the height of the desmin filaments upon stretching them (Fig. 4 *C*). This height decrease was larger than expected from a constant volume approximation (Fig. 4 *C*, *dashed line*). Hence we interpreted this behavior as evidence for plastic deformation.

Assuming that the height of a desmin filament adsorbed to mica is proportional to its diameter, we estimated the minimal diameter of a stretched desmin filament to be 3–4 nm instead of 6.8 nm, as expected for a constant volume regime. For comparison, a minimal diameter of 3–4 nm was also measured on TEM images of sheared desmin networks (Fig. 7 *B*). Based on the tensile force applied to a filament at 240% extension, i.e., 3.4 nN (Fig. 5 *A*) and compensating for the effect of friction, we estimated the tensile strength of a single desmin IF to be in the range of 240–420 MPa. By contrast, by assuming a constant volume approximation, we obtained a value of 90 MPa (Fig. 6, *filled black circles*). The only other ''pure'' IF system for which tensile properties where estimated is the μm-wide hagfish slime thread made of keratin-like IFs (14). In that case, only the engineering stress, which is the force divided by the cross sectional area of the slime thread before stretching, was measured, yielding a tensile strength of 180 $\pm$ 20 MPa (14). This is sixfold higher than our estimate of the engineering tensile strength for desmin filaments, i.e., 28 MPa. This difference might arise primarily from the cohesive interaction between keratin-like IFs within the slime thread.

Based on our AFM data we estimate the onset of ''plastic'' deformation, as defined by a decrease in the filament's volume at 50%–100% extension (Fig. 6). In that range, the stress-strain curve obtained using H_S/H_0 (Fig. 6, *filled gray diamonds*) and that obtained from a constant volume approximation (Fig. 6, *filled black circles*) separate. This corresponds to extensions for which the α-helix to β-sheet transition has been observed in strained keratin fibers (14,15). However an irreversible length change was reported to have occurred at 30% extension for the same fibers (14,15).

Hence, we hypothesize that above 50%–100% extension, the tensile properties of desmin IFs are dominated by a plastic deformation. Morphologically, this corresponds to the appearance of a neck region of small diameter (Figs. 7 and 8, *step 4*) and to an exponential increase in the stress with the extension (Fig. 6, *gray curve*). This response of a filament to deformation is named ''strain hardening''. Furthermore, we

propose that the plastic deformation corresponds to the unfolding of the α-helical coiled-coil dimers, as seen for hagfish slime threads (14). Similarly, a fully stretched desmin filament is supposed to contain chains in a mainly β-sheet form, similar to the one characterized in stretched keratin fibers by x-ray diffraction (14,15). The structure of a fully stretched desmin filament containing on average 45 monomers in cross section could then be approximated by a crystalline packing of five β-sheets containing nine strands each. Based on an interstrand spacing of 0.47 nm and an intersheet spacing of 0.95 nm (27), we obtain a filament with a rectangular 3.7 nm $\times$ 4.7 nm cross section. These values are in good agreement with the TEM pictures of sheared desmin networks (Fig. 7).

Tensile properties of desmin IFs in authentic muscle fibers

Several groups have reported the tensile properties of KCl/KI-treated muscle fibers from which most of the actin and myosin filaments had been removed. The measured stress-strain curves were attributed to the longitudinal desmin filaments connecting successive Z-disks along each myofibril (28,29). This interpretation was based on EM investigations of fibers before and after treatment (4,6).

For both single rat cardiac myocytes (29) and skinned rabbit muscle fibers (28), the stress-strain curves after treatment were nonlinear with a strain-hardening region above 80%–100% extension very similar to the one obtained with single desmin IFs (Fig. 6). Hence, we may employ the data obtained by our measurements to estimate the number of desmin filaments that may bear the tension. For example, a cardiac myocyte treated with KCl/KI and stretched to 190% extension generated a passive tension of 140 kPa (29) compared to 120 MPa for a single filament (Fig. 6). Since these myocytes had a cross section of $\sim$180 μm^2, $\sim$15,000 desmin filaments would have to be aligned with the myocyte's main axis. Assuming an average myofibril diameter of 1 μm (4), we estimated the number of myofibrils per myocyte to be $\sim$230. Hence, each myofibril should be surrounded by $\sim$65 desmin filaments. A similar number, i.e., 50–100, was estimated for skeletal muscle myofibrils based on TEM pictures of KCl/KI-treated fibers (6).

Both the in vivo and the in vitro data indicate that the longitudinal desmin IFs contribute to passive muscle tension above a 100% extension of the sarcomeres. In the case of intact sarcomeres, other stress-bearing elements, such as titin, prevent such large deformations to happen. However, if a sarcomere's actomyosin framework becomes damaged then the desmin IFs are the only remaining mechanical elements between successive Z-disks. Desmin IFs would then extend to their limit to protect a damaged sarcomere from the tension generated by surrounding contractile sarcomeres (28,29). Overstretched desmin IFs may become more susceptible to calpain proteolysis, thus explaining the localized degradation of desmin in muscles exposed to eccentric contraction (30).

Although the tensile properties of single desmin IFs can be used to get a better understanding of the mechanical role of these filaments within muscles, many questions remain. For example, what is the influence of binding proteins, such as the chaperon αB-crystallin (31), on desmin filament mechanics? In particular, it would be interesting to find out if some chaperons prevent the unfolding of the desmin dimers at large extension (see previous section).

CONCLUSION

In this study, we qualitatively measured the tensile properties of single desmin IFs. Our results are in good agreement with the tensile properties measured with macroscopic bundles of keratin-like IFs and desmin-IFs containing extracted muscle fibers. Based on these findings, it is likely that other IFs will exhibit a similar propensity to strain harden at large deformations. Most importantly, the stress-strain curve of pure, in vitro reassembled desmin IFs determined in this study (Fig. 6), rather than being taken literally, should be considered as a qualitative representation of what happens in situ, for example, in intact cells and tissues. The in vivo situation is complicated by the presence of many IF-associated proteins that are bound to the surface of the filaments by phosphorylation (32) that may locally ''soften'' the filaments and by the presence of more than one type of IF protein in some of the filaments. Nevertheless, our AFM-based nanomechanical approach offers the unique possibility to dissect at the molecular, single-filament level the influence of such factors as well as the influence of disease-causing point mutations in IF proteins (33).

We thank Drs. Roderick Lim, Patrick Frederix, Enrico Gnecco, and Ernst Meyer for fruitful discussions.

H.H acknowledges support from the German Research Foundation (DFG grant number HE 1853/4-3). U.A. and H.H. acknowledge the support by the European Commission (Contract LSHM-CT-2005-018690). L.K. was supported by a grant from the Swiss Society for Research on Muscular Diseases awarded to U.A. and Sergei Strelkov. This work was also supported by funds from the National Center of Competence in Research in Nanoscale Science (NCCR-Nano), an IF grant from the Swiss National Science Foundation, and funds from the Canton Basel-Stadt and the M. E. Müller Foundation of Switzerland, all awarded to U.A.

REFERENCES

1. Strelkov, S. V., H. Herrmann, and U. Aebi. 2003. Molecular architecture of intermediate filaments. *Bioessays.* 25:243–251.
2. Omary, M. B., P. A. Coulombe, and W. H. McLean. 2004. Intermediate filament proteins and their associated diseases. *N. Engl. J. Med.* 351:2087–2100.
3. Capetanaki, Y., R. J. Bloch, A. Kouloumenta, M. Mavroidis, and S. Psarras. 2007. Muscle intermediate filaments and their links to membranes and membranous organelles. *Exp. Cell Res.* 313:2063–2076.
4. Granger, B. L., and E. Lazarides. 1979. Desmin and vimentin coexist at the periphery of the myofibril Z disc. *Cell.* 18:1053–1063.
5. Shah, S. B., J. Davis, N. Weisleder, I. Kostavassili, A. D. McCulloch, E. Ralston, Y. Capetanaki, and R. L. Lieber. 2004. Structural and functional roles of desmin in mouse skeletal muscle during passive deformation. *Biophys. J.* 86:2993–3008.

6. Wang, K., and R. Ramirez-Mitchell. 1983. A network of transverse and longitudinal intermediate filaments is associated with sarcomeres of adult vertebrate skeletal muscle. *J. Cell Biol.* 96:562–570.
7. Lazarides, E., and B. D. Hubbard. 1976. Immunological characterization of the 100 Å filaments from muscle cells. *Proc. Natl. Acad. Sci. USA.* 73:4344–4348.
8. Herrmann, H., H. Bär, L. Kreplak, S. V. Strelkov, and U. Aebi. 2007. Intermediate filaments: from cell architecture to nanomechanics. *Nat. Rev. Mol. Cell Biol.* 8:562–573.
9. Sam, M., S. Shah, J. Friden, D. J. Milner, Y. Capetanaki, and R. L. Lieber. 2000. Desmin knockout muscles generate lower stress and are less vulnerable to injury compared with wild-type muscles. *Am. J. Physiol. Cell Physiol.* 279:1116–1122.
10. Li, Z., M. Mericskay, O. Agbulut, G. Butler-Browne, L. Carlsson, L. E. Thornell, C. Babinet, and D. Paulin. 1997. Desmin is essential for the tensile strength and integrity of myofibrils but not for myogenic commitment, differentiation, and fusion of skeletal muscle. *J. Cell Biol.* 139:129–144.
11. Kreplak, L., and D. S. Fudge. 2007. Biomechanical properties of intermediate filaments: from tissues to single filaments and back. *Bioessays.* 29:26–35.
12. Mücke, N., L. Kreplak, R. Kirmse, T. Wedig, H. Herrmann, U. Aebi, and J. Langowski. 2004. Assessing the flexibility of intermediate filaments by atomic force microscopy. *J. Mol. Biol.* 335:1241–1250.
13. Kreplak, L., H. Bär, J. F. Leterrier, H. Herrmann, and U. Aebi. 2005. Exploring the mechanical behavior of single intermediate filaments. *J. Mol. Biol.* 354:569–577.
14. Fudge, D. S., K. H. Gardner, V. T. Forsyth, C. Riekel, and J. M. Gosline. 2003. The mechanical properties of hydrated intermediate filaments: insights from hagfish slime threads. *Biophys. J.* 85:2015–2027.
15. Kreplak, L., J. Doucet, P. Dumas, and F. Briki. 2004. New aspects of the α-helix to β-sheet transition in stretched hard α-keratin fibers. *Biophys. J.* 87:640–647.
16. Herrmann, H., I. Hofmann, and W. W. Franke. 1992. Identification of a nonapeptide motif in the vimentin head domain involved in intermediate filament assembly. *J. Mol. Biol.* 223:637–650.
17. Bär, H., N. Mücke, P. Ringler, S. A. Müller, L. Kreplak, H. A. Katus, U. Aebi, and H. Herrmann. 2006. Impact of disease mutations on the desmin filament assembly process. *J. Mol. Biol.* 360:1031–1042.
18. Sader, J. E., I. Larson, P. Mulvaney, and L. R. White. 1995. Method for the calibration of atomic-force microscope cantilevers. *Rev. Sci. Instrum.* 66:3789–3798.
19. Nonnenmacher, M., J. Greschner, O. Wolter, and R. Kassing. 1996. Scanning force microscopy with micromachined silicon sensors. *J. Vac. Sci. Technol. B.* 9:1358–1362.
20. Mücke, N., R. Kirmse, T. Wedig, J. F. Leterrier, and L. Kreplak. 2005. Investigation of the morphology of intermediate filaments adsorbed to different solid supports. *J. Struct. Biol.* 150:268–276.
21. Guzman, C., S. Jeney, L. Kreplak, S. Kasas, A. J. Kulik, U. Aebi, and L. Forro. 2006. Exploring the mechanical properties of single vimentin intermediate filaments by atomic force microscopy. *J. Mol. Biol.* 360:623–630.
22. Heidelberg, A., L. T. Ngo, B. Wu, M. A. Phillips, S. Sharma, T. I. Kamins, J. E. Sader, and J. J. Boland. 2006. A generalized description of the elastic properties of nanowires. *Nano Lett.* 6:1101–1106.
23. Falvo, M. R., S. Washburn, R. Superfine, M. Finch, F. P. Brooks Jr., V. Chi, and R. M. Taylor. 1997. Manipulation of individual viruses: friction and mechanical properties. *Biophys. J.* 72:1396–1403.
24. Landau, L. D., and E. M. Lifshitz. 1970. Theory of Elasticity. Pergamon, Oxford.
25. Tsuda, Y., H. Yasutake, A. Ishijima, and T. Yanagida. 1996. Torsional rigidity of single actin filaments and actin-actin bond breaking force under torsion measured directly by in vitro micromanipulation. *Proc. Natl. Acad. Sci. USA.* 93:12937–12942.
26. Fudge, D. S., and J. M. Gosline. 2004. Molecular design of the α-keratin composite: insights from a matrix-free model, hagfish slime threads. *Proc. Biol. Sci.* 271:291–299.
27. Fraser, R. D. B., T. P. MacRae, D. A. D. Parry, and E. Suzuki. 1969. Structure of β-keratin. *Polymer (Guildf.).* 10:810–826.
28. Wang, K., R. McCarter, J. Wright, J. Beverly, and R. Ramirez-Mitchell. 1993. Viscoelasticity of the sarcomere matrix of skeletal muscles. The titin-myosin composite filament is a dual stage molecular spring. *Biophys. J.* 64:1161–1177.
29. Granzier, H. L., and T. Irving. 1995. Passive tension in cardiac muscle: contribution of collagen, titin, microtubules and intermediate filaments. *Biophys. J.* 68:1027–1044.
30. Lieber, R. L., L. E. Thornell, and J. Friden. 1996. Muscle cytoskeletal disruption occurs within the first 15 min of cyclic eccentric contraction. *J. Appl. Physiol.* 80:278–284.
31. Perng, M. D., S. F. Wen, P. van den Ijssel, A. R. Prescott, and R. A. Quinlan. 2004. Desmin aggregate formation by R120G αB-crystallin is caused by altered filament interactions and is dependent upon network status in cells. *Mol. Biol. Cell.* 15:2335–2346.
32. Inagaki, M., Y. Nishi, K. Nishizawa, M. Matsuyama, and C. Sato. 1987. Site-specific phosphorylation induces disassembly of vimentin filaments in vitro. *Nature.* 328:649–652.
33. Bär, H., N. Mücke, A. Kostareva, G. Sjoberg, U. Aebi, and H. Herrmann. 2005. Severe muscle disease-causing desmin mutations interfere with in vitro filament assembly at distinct stages. *Proc. Natl. Acad. Sci. USA.* 102:15099–15104.